Carbon sequestration in the deep Atlantic enhanced by Saharan dust

Katsiaryna Pabortsava[1,*], Richard S. Lampitt[1], Jeff Benson[1], Christian Crowe[1], Robert McLachlan[1], Frederic A. C. Le Moigne[2], C. Mark Moore[3], Corinne Pebody[1], Paul Provost[1], Andrew Rees[4], Gavin Tilstone[4], E. Malcom S. Woodward[4]

[1] National Oceanography Centre, European Way, Southampton, UK

[2]GEOMAR Helmholtz Centre for Ocean Research, Kiel, Germany

[3]Ocean and Earth Science, University of Southampton, Waterfront Campus, European Way, Southampton, UK

[4]Plymouth Marine Laboratory, Plymouth, UK

Enhanced atmospheric input of dust-borne nutrients and minerals to the remote surface ocean can potentially increase carbon uptake and sequestration at depth. Nutrients can enhance primary productivity, and mineral particles act as ballast, increasing sinking rates of particulate organic matter. Here we present a unique 2-year time-series of sediment-trap observations of particulate organic carbon flux to 3000 m depth, measured directly in two locations: the dust-rich central North Atlantic gyre and the dust-poor South Atlantic gyre. We find that carbon fluxes are twice as high and a higher proportion of primary production is exported to depth in the dust-rich North Atlantic gyre. Low stable nitrogen isotope ratios suggest that high fluxes result from the stimulation of nitrogen fixation and productivity following the deposition of dust-borne nutrients. Sediment traps in the northern gyre also collected intact colonies of nitrogen-fixing *Trichodesmium* species. Whereas ballast in the southern gyre is predominantly biogenic, dust-derived mineral particles constitute the dominant ballast element during the enhanced carbon fluxes in the northern gyre. We conclude that dust deposition increases

carbon sequestration in the North Atlantic gyre through the fertilisation of the nitrogen-fixing community in surface waters and mineral ballasting of sinking particles.

Flux of airborne desert dust into the surface ocean can increase the amount of photosynthetically fixed carbon dioxide (CO_2) by reducing nutrient limitation of primary production and thus increase the flux of particulate organic carbon (POC) to the deep ocean[1]. Dense dust-derived lithogenic particles can also increase particle size through aggregation and enhance sinking velocity and preservation of POC through ballasting, allowing more carbon to penetrate deeper into the ocean's interior[2]. The impact of dust input on downward POC flux can be especially important in the subtropical low-nutrient low-chlorophyll (oligotrophic) gyres which occupy 60% of the global ocean surface[3] and thus are likely large sinks for atmospheric CO_2. Even relatively small changes in downward POC flux in these immense areas would significantly affect the global carbon budget. However, the transport of organic carbon (*i.e.* Biological Carbon Pump) in oligotrophic regions is very poorly understood, and large uncertainties remain over the impact of enhanced dust deposition on the magnitude of POC flux below the depth of winter mixing (sequestration).

We tested the hypothesis that enhanced dust deposition increases POC sequestration in remote low-nutrient low-chlorophyll provinces by directly measuring downward deep POC flux in the centres of the subtropical North and South Atlantic gyres. The study regions represent permanently stratified systems characterised by restricted nutrient advection, and hence extremely low surface concentrations of macronutrients (nitrate and phosphate) and chlorophyll. Here, picoplankton dominate community structure[4], while heterotrophic bacteria and cyanobacteria govern ecosystem metabolism, channelling a large proportion of POC into the microbial loop[5], thus diminishing its export out of the euphotic zone. The subtropical North Atlantic, however, receives large depositional fluxes of Saharan dust with associated essential nutrients (e.g. nitrogen, phosphorus, iron)[1] blocked from the South Atlantic region by the Inter-

Tropical Convergence Zone[6]. The Fe-rich surface waters of the northern gyre are favoured by N_2 fixing microbes (diazotrophs) that generate bioavailable nitrogen for other phytoplankton[7], thereby allowing for a higher proportion of primary production to be converted into sinking POC than would otherwise occur. Phosphate co-limits the Fe-induced N_2 fixation and production fuelled by atmospheric nitrogen[8, 9]. This can exert an important control over the amount of POC ultimately produced from diazotrophic and atmospheric sources and subsequently available for export. Along with this fertilisation effect, increased lithogenic particle concentration following dust input can also facilitate POC flux to depth through additional incorporation of dense dust particles[10]. Biomineral ballasting is otherwise regulated by calcite which is typically found in both gyres[11]. However, the degree to which lithogenic ballasting can drive the increased POC sedimentation would itself be limited by the amount of POC present[12].

Field observations in the central Atlantic gyres

We directly captured POC flux in the central Atlantic gyres from 2007 to 2010 using sediment traps moored at 3000 m depth at sites NOG (23°N 41°W) and SOG (18°S 25°W) (Fig.1). During this period, NOG was subjected to, on average, ten-fold higher dust deposition compared to SOG (Fig. 2a), as inferred from dust concentration measurements over Barbados[13] for NOG and modelled data[14, 15] for SOG (Methods). At both sites, the average surface production rates derived from a Vertically Generalised Production Model (VGPM)[16] were lower than much of the global ocean[17], and on average 23% higher at NOG than at SOG (Fig. 2b). The observed POC fluxes to the trap at NOG (0.40-2.7 mg C m^{-2} $d^{-1;}$ mean =1.06 mg C m^{-2} d^{-1}) were always at least two-fold higher than at SOG (0.21-0.95 mg C m^{-2} d^{-1}; mean = 0.49 mg C m^{-2} d^{-1}) (Fig. 2d, 3). The POC fluxes at NOG and SOG were significantly lower than the depth-normalised values reported for the oligotrophic sites in the western North Atlantic gyre (station OFP (BATS))[18] and subtropical North Pacific gyre (station ALOHA)[19], and hence they

are the lowest measured in the global ocean. From the ratios of POC flux to VGPM primary production (both variables were averaged over the trap deployment period) we calculate almost double the fraction of surface production reaching 3000 m depth at NOG (0.60%) compared to SOG (0.37%). These very low values are similar to the records at BATS (0.59%)[18] and imply an overall more efficient downward POC transport in the dusty northern gyre. Lithogenic flux determined from aluminium concentrations in trap material was significantly lower at SOG than at NOG (Fig. 2c) and elsewhere in the subtropical North Atlantic[18, 20], indicating that the inter-basin differences in dust deposition propagated to depth. The NOG data bridge the previous observations of deep lithogenic flux in the eastern and western parts of the northern gyre[18, 20] showing the westward gradient of decreasing deep lithogenic fluxes driven by the weakening of the Saharan dust transport towards the northwest-Atlantic[13].

Although higher at NOG, at both sites, POC flux was enhanced during late summer-autumn (>120% of the annual mean value; Fig. 3), a period of warm sea-surface temperature (25.0 - 28.2 °C), relatively shallow mixed layer (<50 m), and low surface chlorophyll concentrations (<0.04 mg m^{-3}; Supplementary Fig. 1). At NOG, the average dust input during summer-autumn (14.4±8.9 mg m^{-2} d^{-1}) exceeded the wintertime values (8.87±11.6 mg m^{-2} d^{-1}) (Fig. 3a). An enhanced input of dust-borne nitrogen, phosphorus and iron has likely occurred during this period. After nitrogen is exhausted by the dust-stimulated primary producers, the warm and strongly stratified water column would offer optimal conditions for enhanced N_2 fixation provided there is enough iron and phosphate present to satisfy cellular demands of diazotrophs[7, 8, 9]. Bloom-forming *Trichodesmium* spp. dominate diazotrophic biomass in the region of NOG[21]. Elevated N_2 fixation rates by these diazotrophs were reported during summer-autumn (median 34.9 µmol N m^{-2} d^{-1}) compared to winter-spring (median 12.2 µmol N m^{-2} d^{-1}) (refs[21, 22, 23, 24, 25]). This coincides with higher fluxes of aerosol iron in autumn than in spring[26] and higher surface concentrations of dissolved iron in the early autumn[27] (1.0-1.3

nmol L^{-1}) than in winter[28] (0.18-0.54 nmol L^{-1}). Lower phosphate concentrations measured in the central northern gyre during summer have also been attributed to the enhanced diazotrophic activity exhausting the phosphate pool[8]. Remarkably, we find a strikingly high POC flux of up to 2.7 mg C m^{-2} d^{-1} in August-September 2009 at NOG (Fig. 3a). This relatively short POC export pulse, never seen at SOG, accounted for 29% of total POC sequestered at NOG during 2007-2009 and greatly exceeded the mean wintertime POC flux at NOG (0.88±0.13 mg C m^{-2} d^{-1}) and the daily flux at SOG. A notable presence of some intact *Trichodesmium* "tufts" (Figs. 3a, 4) within this pulse suggests a potential involvement of these diazotrophs in driving the extreme POC sequestration event at NOG. Similarly short and efficient POC export pulses to > 2800 m depth have been regularly observed at ALOHA following a summertime increase in productivity and biomass of diatom-diazotroph symbiotic phytoplankton[19].

Fertilisation effect of dust

We measured markedly low stable nitrogen isotope ratios in the trap material ($\delta^{15}N_{PN}$, in ‰ relative to air) from the dust-rich NOG (range 0.40-1.32‰; mass-weighed mean 0.77‰), indicating that isotopically light nitrogen introduced by enhanced N_2 fixation and potentially atmospheric deposition[29] significantly contributed to sinking particles. Some of this low $\delta^{15}N$ signal might have originated south of NOG (10º-16ºN), before being transported to and accumulated at the NOG thermocline as low $\delta^{15}N_{nitrate}$ during northward water mass transit[7, 30]. However, a strong inverse correlation between $\delta^{15}N_{PN}$ and POC flux (R^2=0.67, p=0.001) with *Trichodesmium* "tufts" present at the lowest $\delta^{15}N_{PN}$ values (Figs. 4, 5), is suggestive of a direct link between elevated POC flux at NOG and a local supply of newly fixed nitrogen by diazotrophs whose activity was likely stimulated by substantial inputs of dust-borne iron and phosphorus. Observations at NOG are qualitatively similar to those at ALOHA[19], where $\delta^{15}N_{PN}$ minima and diazotroph-driven particulate POC flux maxima are closely associated. Dust

deposition, which is a substantial source of isotopically light nitrogen in the region (8.5 μmol m^{-2} d^{-1}; ref[31]) could augment the deep POC flux lowering its $\delta^{15}N$ signature.

In contrast to NOG, sinking particles from the dust-poor SOG carried significantly heavier $\delta^{15}N_{PN}$ of 3.70‰ to 4.41‰ (mass-weighted mean 4.07‰). This is similar to the oceanic average $\delta^{15}N$ of deep-water nitrate (4.8‰; ref[29]), and hence this source was probably fuelling primary production at SOG.

The deep $\delta^{15}N_{PN}$ at NOG and SOG fit a broad range of $\delta^{15}N$ values reported for particulate nitrogen in the upper waters of the central North and South Atlantic gyres[32, 33] (Supplementary Fig. 2). At both sites, trap material was ^{15}N-enriched compared to the particles suspended in the euphotic zone (top 130 m) likely due to fractionation resulting from remineralisation processes in both the surface and mesopelagic (Ref 34). Similar $\delta^{15}N$ values for trap material and particles from 150-160 m depth may also point to a potentially important contribution of heavier $\delta^{15}N$ signal formed at the deep chlorophyll maximum to $\delta^{15}N_{PN}$.

We estimated the contribution of different nitrogen sources to $\delta^{15}N_{PN}$ at NOG and SOG using a two-end member nitrogen mass-balance model[29] (see Methods and references therein). We assumed that the isotope budget of the mixed layer in the permanently oligotrophic gyres incorporates nitrogen supplied by diazotrophs, by vertical diffusion across the nitrate concentration gradient, and from dust (NOG only). We also assumed negligible isotopic fractionation following complete nitrogen assimilation by phytoplankton. The average isotopic signature of diazotrophic biomass (-1±1‰) was used as the N_2 fixation endmember. The upper thermocline nitrate endmember was represented by $\delta^{15}N$-nitrate averaged over the depth of the nitrate gradient spanning the euphotic layer at NOG (2.73±0.36‰) and SOG (6.22±0.35‰). The dust-derived nitrogen endmember was assigned $\delta^{15}N$ of -3.1‰ based on the average isotopic composition of bulk aerosols influenced by Saharan dust. Using these endmember values, we find that local N_2 fixation could contribute on average 50.4±8.4% to the isotopic

signal of nitrogen sequestration at NOG, while aerosol nitrogen alone (if all bioavailable) could account for 32.4±5.4% (Supplementary Table 1). The relative contribution of diazotrophs to $\delta^{15}N_{PN}$ at NOG was higher than that at BATS (33%; at average $\delta^{15}N_{PN}$ =+1‰ (ref[34]) and nitrate $\delta^{15}N$=+2.6‰ (ref[35])) and at ALOHA (range 21-48%; refs[19, 36]), where eddy transfer and lateral advection are important mechanisms of nitrogen supply[36, 37]. At SOG, newly fixed nitrogen contributed a smaller, yet considerable portion of $\delta^{15}N_{PN}$ (29.7±3.1%), possibly owing to the activity of unicellular cyanobacteria, major N_2 fixers in the South Atlantic[7, 21]. We, however, acknowledge a significant uncertainty of these results due to an overall lack of time-resolved $\delta^{15}N$ data for the surface nitrate and dust at the trap sites. Moreover, our budgets did not account for a possible origin of particles from a specific trophic level (*e.g.* faecal pellets) and alteration of $\delta^{15}N_{PN}$ due to isotopic fractionation during particle remineralisation and transformation in the mesopelagic. However, regardless of these uncertainties, the isotope budgets suggest a large systematic difference in the contribution of newly fixed local nitrogen inputs between the North and South Atlantic gyres which likely contriutes to the two-fold inter-basin difference in POC sequestration. Our observations thus set an important quantitative constraint on the downward flux of low $\delta^{15}N$ material sinking to the subtropical North Atlantic. They provide compelling evidence for the origin of an isotopically light nitrate reservoir in the subtropical North Atlantic supporting previous observations (e.g. ref[30]).

The unique presence of intact *Trichodesmium* colonies in the deep particles at NOG (Fig. 4) indicates that *Trichodesmium* biomass is not always lost in the surface waters as previously assumed[38, 39], but can leave the euphotic zone and contribute to POC export. It is possible that the "tufts" reached the abyssal depth at NOG in a rapidly sinking (>200 m d^{-1}) *Trichodesmium* bloom, collapsed through viral lysis or programmed cell death[39]. Since Fe starvation at NOG is unlikely, exhaustion of bioavailable phosphrous[8] during the summer might be major triggers of the bloom collapse. Alternatively, the "tufts" might represent

Trichodesmium populations that migrated towards the phosphocline to "mine" phosphate but were unable to return to the light[40]. Finally, *Trichodesmium* can retain dust particles within their morphologically intricate colonies to accelerate Fe dissolution from dust[41]. Trapped dust particles may therefore "ballast" *Trichodesmium* colonies, increasing their density and allowing them to sink rapidly to depth and avoid remineralisation or grazing. This could partly explain the temporal coherence between low $\delta^{15}N$, elevated dust, POC, and lithogenic fluxes during late summer at NOG (Fig. 3a).

Ballasting effect of dust

Higher dust input significantly altered the composition of particles at NOG compared to SOG (Fig. 2e). Dust-derived lithogenic material was the second largest contributor (34.3±11.6%) to the total mass at NOG after calcite, whereas at SOG this value was 4.7±2.3%, consistent with the difference in the amount of dust being deposited at each site (Fig. 2a). Although the seasonal signal of elevated dust flux at both sites was largely lost at 3000 m depth, we still observed elevated lithogenic flux at NOG (>120% of the annual average) in winter 2008 and summer-autumn 2008 and 2009 concurrently with the increased POC flux and following high dust input (Fig. 3a). Assuming that this temporal coherence was not accidental, we investigated the relative involvement of lithogenic and biogenic (opal + calcite) ballast phases in enhanced POC sequestration. Based on the outputs of the mineral-associated POC flux model and multiple linear regression analysis[2, 42] (Methods), 41.0% of POC flux at SOG was ballasted by lithogenic material. This, however, might be an overestimation driven by a relatively large carrying coefficient for lithogenic ballast (0.371) which resulted from a nearly 1:1 ratio of POC to lithogenic flux and their strong positive correlation (Spearman's p=0.91). At NOG the percentage of POC ballasted by lithogenic particles increased from 45.7% during low POC flux to 70.1% during high flux in the summer-autumn (Supplementary Table 2). Overall, lithogenic material appears to be a more important ballast for POC in the central

northern gyre compared to its western boundary (25%), where lithogenic fluxes are lower and opal fluxes are ten times higher[18]. We suggest that at NOG elevated dust inputs may shift the dominant ballasting phase from biogenic to lithogenic, increasing POC flux to the deep ocean. This is likely achieved through a sudden increase in mineral particle concentration following dust deposition and subsequent stimulation of aggregation of organic matter, including that of diazotrophs, in the surface waters[10]. Moreover, clay particles, constituting >60% of the aerosol dust over the central North Atlantic[43], are denser (2.79 g cm^{-3}) than biomineral calcite (2.65 g cm^{-3}) and opal (2.1 g cm^{-3}), and thus would likely increase sinking velocity of POC upon aggregation. Although currently debated in the literature (e.g. refs.[44, 45]), lithogenic ballast might have also exert an enhanced protective effect on POC compared to calcite. Recent laboratory experiments[45, 46] demonstrated slower degradation rates for clay-ballasted POC relative to calcite-ballasted POC. The existence of such protective effect of lithogenic material is yet to be shown in the field.

Mechanism of dust-induced enhancement of carbon sequestration

Lithogenic particles did not represent the main ballasting phase for POC during periods of high and low lithogenic fluxes and were not associated with the biomineral fluxes at NOG (Supplementary Table 2). The ballasting ability of lithogenic particles at NOG appears to be confined to the summer-autumn period (Fig. 3a) when the surface fertilisation by dust was potentially the strongest. This tight temporal coupling suggests that the presence of additional fresh organic (i.e. fertilisation effect) matter might be required to activate effective lithogenic ballasting while lithogenic particles are critical to transport the fertilisation effect to the deep ocean. The variability in mineralogy and morphology of dust arriving at NOG from different locations in the Sahara during winter[47] and summer may have also impacted both fertilisation and ballasting properties of dust.

Overall, enhanced POC sequestration in the dust-rich NOG suggests that in the vast nutrient-limited Atlantic, the strength of the biological carbon pump could be significantly lower without concurrent dust-induced fertilisation and ballasting. The observed two-fold enhancement of POC sequestration under a ten-fold higher dust (iron) input at NOG further points to a potentially important role of phosphate in setting the upper bound for the Fe-driven enhancement of POC export. However, fertilisation could also stimulate the activity of heterotrophic bacteria, increasing remineralisation and a corresponding reduction of carbon export[5].

Under the current climatic trends, the subtropical oligotrophic gyres are predicted to expand over the coming centuries[48]. Multi-decadal observations of dust concentrations over Barbados have already revealed a weakening of dust transport from North Africa to the North Atlantic as a function of increasing sea-surface temperature[13]. Predicted changes in wind patterns are expected to continue altering dust deposition into the ocean and hence input of nutrients and mineral ballast[49]. In parallel, ongoing ocean acidification might affect bioavailability of essential nutrients, including iron[50]. All these perturbations will certainly alter POC sequestration in the oligotrophic gyres, and hence global climate, in the coming centuries. Therefore, our study urges for a better understanding of the present Biological Carbon Pump functioning in the nutrient-limited oceans.

References

1. Jickells, T., An, Z., Andersen, K. K., Baker, A., Bergametti, G., Brooks, N., *et al.* Global iron connections between desert dust, ocean biogeochemistry, and climate. *Science* **308**(5718)**:** 67-71 (2005).

2. Klaas, C., Archer, D.E. Association of sinking organic matter with various types of mineral ballast in the deep sea: Implications for the rain ratio. *Glob. Biogeochem. Cycles* **16**(4)**:** 63-61-63-14 (2002).

3. Antoine, D., André, J.M., Morel, A. Oceanic primary production: 2. Estimation at global scale from satellite (coastal zone color scanner) chlorophyll. *Glob. Biogeochem. Cycles* **10**(1)**:** 57-69 (1996).

4. Zubkov, M.V., Sleigh, M.A., Tarran, G.A., Burkill, P.H., Leakey, R.J. Picoplanktonic community structure on an Atlantic transect from 50° N to 50° S. *Deep-Sea Res. Pt. I* **45**(8)**:** 1339-1355 (1998).

5. Marañón, E., Fernández, A., Mourino-Carballido, B., Martinez-Garcia, S., Teira, E., Cermeno, P., *et al.* Degree of oligotrophy controls the response of microbial plankton to Saharan dust. *Limnol. Oceanogr.* **55**(6)**:** 2339-2352 (2010).

6. Schlosser, C., Klar, J.K., Wake, B.D., Snow, J.T., Honey, D.J., Woodward, E.M.S., *et al.* Seasonal ITCZ migration dynamically controls the location of the (sub) tropical Atlantic biogeochemical divide. *P. Natl. Acad. Sci. US* **111**(4)**:** 1438-1442 (2014).

7. Moore, C.M., Mills, M.M., Achterberg, E.P., Geider, R.J., LaRoche, J., Lucas, M.I., *et al.* Large-scale distribution of Atlantic nitrogen fixation controlled by iron availability. *Nat. Geosci.* **2**(12)**:** 867-871 (2009).

8. Mather, R.L., Reynolds, S.E., Wolff, G.A., Williams, R.G., Torres-Valdes, S., Woodward, E.M.S., *et al.* Phosphorus cycling in the North and South Atlantic Ocean subtropical gyres. *Nat. Geosci.* **1**(7)**:** 439-443 (2008).

9. Mills, M.M., Ridame, C., Davey, M., La Roche, J., Geider, RJ. Iron and phosphorus co-limit nitrogen fixation in the eastern tropical North Atlantic. *Nature* **429**(6989)**:** 292-294 (2004).

10. Lee, C., Peterson, M.L., Wakeham, S.G., Armstrong, R.A., Cochran, J.K., Miquel, J.C., *et al.* Particulate organic matter and ballast fluxes measured using time-series and settling velocity sediment traps in the northwestern Mediterranean Sea. *Deep-Sea Res Pt. II* **56**(18)**:** 1420-1436 (2009).

11. Poulton, A.J., Adey, T.R., Balch, W.M., Holligan, P.M. Relating coccolithophore calcification rates to phytoplankton community dynamics: regional differences and implications for carbon export. *Deep-Sea Res Pt. II* **54**(5)**:** 538-557 (2007).

12. Passow, U., De La Rocha, C.L. Accumulation of mineral ballast on organic aggregates. *Glob. Biogeochem. Cycles* **20**(1) (2006).

13. Prospero, J.M., Collard, F.-X., Molinié, J., Jeannot, A. Characterizing the annual cycle of African dust transport to the Caribbean Basin and South America and its impact on the environment and air quality. *Glob. Biogeochem. Cycles* **28**(7)**:** 757-773 (2014).

14. Mahowald, N., Luo, C., Del Corral, J., Zender, C.S. Interannual variability in atmospheric mineral aerosols from a 22-year model simulation and observational data. *J. Geophys. Res.-Atmos.(1984–2012)* **108** (D12) (2003).

15. Luo, C., Mahowald, N.M., Del Corral, J. Sensitivity study of meteorological parameters on mineral aerosol mobilization, transport, and distribution. *Journal of J. Geophys. Res.-Atmos. (1984–2012)* **108** (D15) (2003).

16. Behrenfeld, M.J., Falkowski, P.G. Photosynthetic rates derived from satellite-based chlorophyll concentration. *Limnol. Oceanogr.* **42**(1)**:** 1-20 (1997).

17. Emerson, S. Annual net community production and the biological carbon flux in the ocean. *Glob. Biogeochem. Cycles* **28**(1)**:** 14-28 (2014).

18. Conte, M.H., Ralph, N., Ross, E.H. Seasonal and interannual variability in deep ocean particle fluxes at the Oceanic Flux Program (OFP)/Bermuda Atlantic Time Series (BATS) site in the western Sargasso Sea near Bermuda. *Deep-Sea Res Pt. II* **48**(8–9)**:** 1471-1505 (2001).

19. Karl, D.M,, Church, M.J., Dore, J.E., Letelier, R.M., Mahaffey, C. Predictable and efficient carbon sequestration in the North Pacific Ocean supported by symbiotic nitrogen fixation. *P. Natl. Acad. Sci. US* **109**(6)**:** 1842-1849 (2012).

20. Bory, A., Jeandel, C., Leblond, N., Vangriesheim, A., Khripounoff, A., Beaufort, L., *et al.* Downward particle fluxes within different productivity regimes off the Mauritanian upwelling zone (EUMELI program). *Deep-Sea Res Pt. I* **48**(10)**:** 2251-2282 (2001).

21. Luo, Y.-W., Doney, S., Anderson, L., Benavides, M., Berman-Frank, I., Bode, A., *et al.* Database of diazotrophs in global ocean: abundance, biomass and nitrogen fixation rates. *Earth Syst. Sci. Data* **4**(1)**:** 47-73 (2012).

22. Rees, A. Rates of nitrogen fixation in surface waters by stable-isotope mass spectrometry during the AMT programme cruise AMT20 (JC053). British Oceanographic Data Centre - Natural Environment Research Council, UK (2015). doi:10.5285/215a1e9b-428b-52f5-e053-6c86abc06d17.

23. Painter, S. Nitrogen fixation from vertical profiles from CTD rosette samples by mass spectrometry on RRS Discovery Cruise D369. British Oceanographic Data Centre - Natural Environment Research Council, UK (2015). doi:10.5285/183e535a-00c2-21a3-e053-6c86abc0b1a5.

24. Snow, J.M., Moore, C.M. Rates of nitrogen fixation in surface waters by stable-isotope mass spectrometry during the AMT programme cruise AMT21 (D371). British

Oceanographic Data Centre - Natural Environment Research Council, UK (2015). doi:10.5285/1b0ebfb2-42b8-3c96-e053-6c86abc02677.

25. Honey, D.J., Gledhill, M., Achterberg, E.P. Nitrogen Fixation from vertical CTD profile rosette samples by stable-isotope mass spectrometry on cruise D346. British Oceanographic Data Centre - Natural Environment Research Council, UK (2016). doi:10.5285/215bc997-af14-1c58-e053-6c86abc09652.

26. Baker, A.R., Adams, C., Bell, T.G., Jickells, T.D., Ganzeveld, L. Estimation of atmospheric nutrient inputs to the Atlantic Ocean from 50°N to 50°S based on large-scale field sampling: Iron and other dust-associated elements. *Glob. Biogeochem. Cycles* **27**(3)**:** 755-767 (2013).

27. Ussher, S.J., Achterberg, E.P., Powell, C., Baker, A.R., Jickells, T.D., Torres, R., *et al.* Impact of atmospheric deposition on the contrasting iron biogeochemistry of the North and South Atlantic Ocean. *Glob. Biogeochem. Cycles* **27**(4)**:** 1096-1107 (2013).

28. Conway, T.M., John, S.G. Quantification of dissolved iron sources to the North Atlantic Ocean. *Nature* **511**(7508)**:** 212-215 (2014).

29. Montoya, J.P. in *Stable Isotopes in Ecology and Environmental Science, Second Edition* (eds Michener, R. & Lajtha, K.), 176-201 (Blackwell Publishing Ltd., 2007).

30. Knapp, A.N., DiFiore, P.J., Deutsch, C., Sigman, D.M., Lipschultz, F.. Nitrate isotopic composition between Bermuda and Puerto Rico: Implications for N_2 fixation in the Atlantic Ocean. *Glob. Biogeochem. Cycles* **22**(3) (2008).

31. Baker, A., Weston, K., Kelly, S., Voss, M., Streu, P., Cape, J. Dry and wet deposition of nutrients from the tropical Atlantic atmosphere: Links to primary productivity and nitrogen fixation. *Deep-Sea Res. Pt. I* **54**(10)**:** 1704-1720 (2007).

32. Reynolds, S.E., Mather, R.L., Wolff, G.A., Williams, R.G., Landolfi, A., Sanders, R., *et al*. How widespread and important is N_2 fixation in the North Atlantic Ocean? *Glob. Biogeochem. Cycles* **21**(4) (2007).

33. Fernández, A., Marañón, E., Bode, A. Large-scale meridional and zonal variability in the nitrogen isotopic composition of plankton in the Atlantic Ocean. *J. Plankton Res.* **36** (4): 1060-1073 (2014).

34. Altabet, M.A. Variations in nitrogen isotopic composition between sinking and suspended particles: implications for nitrogen cycling and particle transformation in the open ocean. *Deep Sea Res.* **35**(4)**:** 535-554 (1988).

35. Knapp, A.N., Hastings, M.G., Sigman, D.M., Lipschultz, F., Galloway, J.N. The flux and isotopic composition of reduced and total nitrogen in Bermuda rain. *Mar. Chem.* **120**(1)**:** 83-89 (2010).

36. Dore, J.E., Brum, J.R., Tupas, L.M., Karl, D.M. Seasonal and interannual variability in sources of nitrogen supporting export in the oligotrophic subtropical North Pacific Ocean. *Limnol. Oceanogr.* **47**(6)**:** 1595-1607 (2002).

37. Lipschultz, F., Bates, N.R., Carlson, C.A., Hansell, D.A. New production in the Sargasso Sea: History and current status. *Glob. Biogeochem. Cycles* **16**(1)**:** 1-1-1-17 (2002).

38. Thompson, A.W., Zehr, J.P. Cellular interactions: lessons from the nitrogen-fixing cyanobacteria. *J. Phycol.* **49**(6)**:** 1024-1035 (2013).

39. Mulholland M. The fate of nitrogen fixed by diazotrophs in the ocean. *Biogeosciences* **4**(1): 37-51 (2007).

40. Villareal, T., Carpenter, E. Buoyancy regulation and the potential for vertical migration in the oceanic cyanobacterium Trichodesmium. *Microb. Ecol.* **45**(1)**:** 1-10 (2003).

41. Rubin, M., Berman-Frank, I., Shaked, Y. Dust-and mineral-iron utilization by the marine dinitrogen-fixer Trichodesmium. *Nat. Geosci.* **4**(8)**:** 529-534 (2011).

42. Honda, M.C., Watanabe, S. Importance of biogenic opal as ballast of particulate organic carbon (POC) transport and existence of mineral ballast-associated and residual POC in the Western Pacific Subarctic Gyre. *Geophys. Res. Lett.* **37**(2) (2010).

43. Glaccum, R.A., Prospero, J.M. Saharan aerosols over the tropical North Atlantic—Mineralogy. *Mar. geol.* **37**(3)**:** 295-321 (1980).

44. Iversen, M.H., Robert, M.L. Ballasting effects of smectite on aggregate formation and export from a natural plankton community. *Mar. Chem.* **175:** 18-27 (2015).

45. Engel, A., Abramson, L., Szlosek, J., Liu, Z., Stewart, G., Hirschberg, D., *et al.* Investigating the effect of ballasting by $CaCO_3$ in Emiliania huxleyi, II: Decomposition of particulate organic matter. *Deep-Sea Res. Pt II* **56**(18)**:** 1408-1419 (2009).

46. Arnarson, T.S., Keil, R.G. Influence of organic-mineral aggregates on microbial degradation of the dinoflagellate Scrippsiella trochoidea. *Geochim. Cosmochim. Ac.* **69**(8)**:** 2111-2117 (2005).

47. Schepanski, K., Tegen, I., Macke, A. Saharan dust transport and deposition towards the tropical northern Atlantic. *Atmos. Chem. Phys.* **9**(4)**:** 1173-1189 (2009).

48. Polovina, J.J., Howell, E.A., Abecassis, M. Ocean's least productive waters are expanding. *Geophys. Res. Lett.* **35**(3) (2008).

49. Jickells, T., Moore, C.M. The Importance of Atmospheric Deposition for Ocean Productivity. *Annu. Rev. Ecol. Syst.* **46**(1)**:** 481-501 (2015).

50. Sunda, W.G. Iron and the carbon pump. *Science* **327**(5966)**:** 654-655 (2010).

Corresponding author: Correspondence and requests for materials should be addressed to K.P. (katsia@noc.ac.uk).

Acknowledgements: We thank the captains and crew of the *RRS Discovery*, *RRS James Clark Ross* and *RRS James Cook* during cruises D324, D334, JCR186, JCR215 and JC05 for deploying and recovering of the McLane sediment traps. We are grateful to M. Cooper, C. Marsay, P. Martin, A. Moje, P. Statham and M. Stinchcombe for their assistance with laboratory work and advice on analytical and sample-handling issues. We thank J. Prospero for providing the Barbados dust concentration data, N. Mahowald for modelled dust deposition flux data. We thank the British Oceanographic Data Centre and NASA Ocean Colour, and Ocean Productivity website for providing ancillary data. We thank A. Poulton, and R. Sanders for participation in results discussion and feedback on this manuscript. This work is a part of doctoral dissertation of K.P. funded by National Oceanography Centre, Southampton (grant XXXX) and the University of Southampton (grant XXXX). This study is also a contribution to the international IMBER project and was supported by the UK Natural Environment Research Council National Capability funding to Plymouth Marine Laboratory and the National Oceanography Centre, Southampton. This is contribution number 291 of the AMT programme.

Author contributions: K.P. and R.S.L. designed and conducted the research. K.P. analysed the data and wrote the manuscript together with R.S.L. J.B., C.C., R.M., P.P. and C.P. coordinated sediment trap operations, F.A.C.L. and C.M.M. contributed to the interpretation of the results, A.R., G.T. and E.M.S.W. provided the ancillary biogeochemical data.

Additional information: Supplementary information accompanies this paper on www.nature.com/naturegeoscience. Reprints and permissions information is available online at http://npg.nature.com/reprintsandpermissions.

Competing financial interests: The authors declare no competing financial interests.

460 **Figure captions**

461 **Figure 1| Chlorophyll and dust deposition flux in the Atlantic Ocean. a,** annual composite
462 Moderate-resolution Imaging Spectroradiometer chlorophyll-*a* concentration (mg m^{-3}) in 2009.
463 Oligotrophic gyres are represented by dark blue areas of low chlorophyll concentrations (<0.1
464 mg m^{-3}). **b,** basin-wide annually averaged (1974-2004) modelled dust deposition flux re-plotted
465 from ref[14]. Yellow triangles indicate the locations of the NOG and SOG sediment trap
466 moorings, which are also on the annually repeated Atlantic Meridional Transect (AMT) line
467 (www.amt-uk.org). The black solid line shows the AMT-19 cruise track (Oct-Nov 2009)
468 passing through the NOG and SOG sites. Dashed lines indicate an approximate north-south
469 boundary of the Inter-Tropical Convergence Zone.

470 **Figure 2| Surface ocean and deep particle flux data for the study sites. a-d,** mean ± standard
471 deviation values over the respective trap deployment periods. **a,** dust deposition flux (n=25 for
472 NOG and n=26 for SOG). **b**, depth-integrated primary production derived from the
473 chlorophyll-based Vertically Generalised Production Model[16] (Methods) **c,** lithogenic flux
474 (n=40 for both sites). **d,** POC flux (n=40 for both sites). **e**, composition of sediment trap
475 material. The height of the stacked bars represents total particle mass flux.

476 **Figure 3| Time-series fluxes at NOG (a) and SOG (b).** The dust deposition (monthly values)
477 and aluminium-derived lithogenic fluxes are presented on a logarithmic scale. The uncertainty
478 of the dust flux to the South Atlantic is estimated to be at least a factor of 10 (ref[14]). For POC
479 and lithogenic fluxes, the width of each bar corresponds to 14- or 21-day collection interval.
480 Red circles depict stable nitrogen isotopic composition of particles ($\delta^{15}N_{PN}$) from the selected
481 cups. Arrows and a letter "T" indicate the cups where *Trichodesmium* spp. "tufts" were found.
482 Summer-autumn periods are highlighted in yellow.

483

Figure 4| *Trichodesmium* spp. "tufts" from the summer POC flux pulse at NOG. Tufted colonies of *Trichodesmium* spp. cells were identified in the cups collecting in August and September 2009. This is the first record of *Trichodesmium* being exported to bathypelagic depth (>1500 m).

Figure 5| POC flux *vs.* isotopic composition of the trap material ($\delta^{15}N_{PN}$) from NOG (blue circles) and SOG (red circles). The black line is the best fit line of the linear model. Arrows with letter "T" mark the cups where *Trichodesmium* tufts were found. The strong inverse relationship between the magnitude of POC flux and $\delta^{15}N_{PN}$ at NOG signifies a potentially important role of local input of isotopically light N from N_2 fixation (and dust deposition) in enhancing carbon sequestration at this site.

Methods

Particle collection and processing. Sinking particles were collected using 21-cup time-series Parflux Mark 78H–21 sediment traps (McLane Research Laboratories, USA) deployed on a bottom-tethered mooring at a depth of 3000 m in a water depth of >4200 m. At NOG, the traps were deployed from November 4, 2007 to October 5, 2008 and from November 23, 2008 to October 25, 2010, collecting particles over a total of 672 days. At SOG, the traps operated from May 11, 2008 to May 20, 2009 and from May 24, 2009 to June 20, 2010, collecting particles over a total of 766 days. Each trap cup collected for 14 or 21 days. Sample preservative consisted of a solution of sodium chloride (5 g L^{-1}), di-sodium tetra-borate (0.25 g L^{-1}), and formalin (5% vol/vol) made up with deep seawater. Upon recovery, pH was measured and found to be between 8.0 and 8.3. One mL of concentrated formalin solution was then added to the cups to supplement the existing formalin. Sample processing was carried out under dust- and metal-free conditions in a laminar flow cabinet using plastic- or glass-ware only. Prior to all analyses, zooplankton "swimmers" were identified under stereo-microscope (Meiji Techno, Japan) fitted with a photo-camera (Canon EOS-1000, Japan) and handpicked using PTFE-coated tweezers (Dumont, Switzerland) and a plastic pipette (Fisher Scientific, UK). The preservative/particle mixture in each cup was then split into 8 sub-samples using a custom-built rotary PVC splitter. Individual sub-samples from each cup were filtered, dried at 40ºC and analysed for particulate organic carbon, opal, calcite, and trace metals including aluminium. Selected sub-samples were also analysed for stable nitrogen isotope composition.

Chemical analyses of the trap material. Particulate organic carbon (POC) was measured in tin capsules (HEKAtech GmbH) after removing carbonate by *in situ* acidification[51] with concentrated hydrochloric acid and using a high-temperature combustion technique on a CHN analyser (HEKAtech GmbH EURO EA CHNS-O Elemental Analyser) with analytical precision of <0.1%). The median filter blank contribution to POC signal was 2.7%. The

calculated limit of detection (LoD; based on three times standard deviations of the filter blanks) was 8.26 µg (n=20). Particulate Organic Matter (POM) was calculated as 2.2×POC (ref[2]). Splits for calcite were prepared by leaching in 0.4 mol L^{-1} nitric acid with calcium content measured by inductively coupled plasma optical emission spectrometry[52] (Perkin-Elmer Optima 4300DV ICP-OES; analytical precision of <1%). Procedural blanks consisting of unused polycarbonate membranes treated with nitric acid contributed <1% to Ca signal. The LoD of the blank-corrected Ca measurements was wavelength-dependent, ranging from 0.012 to 0.015 µg (n=10). Calcite mass flux was calculated by multiplying calcium-derived flux of particulate inorganic carbon by a factor of 8.3. Samples for opal were digested in 0.2 mol L^{-1} sodium hydroxide, neutralized with 0.1 mol L^{-1} hydrochloric acid and analysed as dissolved silicate on a SEAL QuAATro auto-analyser[52, 53]. The detection limit of the instrument was 0.3 µg. The median contribution of procedural blanks was 3.1%. The LoD of the filter-blank corrected samples was run-dependent ranging from 1.19 to 11.5 µg (n=9). Opal was calculated to be 2.4 × biogenic silica flux assuming 10% water content[52, 53]. Labile and refractory fractions of aluminium in trap material were determined[54]. The labile fraction was extracted with 25% (vol/vol) acetic acid at room temperature, and then the more refractory fraction was fully digested in a mixture of concentrated nitric and hydrofluoric acids at 150°C. The residues of both fractions were redissolved in 0.5 mol L^{-1} nitric acid and analysed by inductively coupled plasma-mass spectrometry (Thermo Fisher Scientific Element 2 XR HR-ICPMS). The LoD of blank corrected aluminium measurements was 0.12 ng g^{-1} (n=10); the concentrations in acid mix and blank filters were 0.764±0.8 ng g^{-1}; (n=10) and 0.843±0.917 ng g^{-1} (n=8), respectively. The accuracy of the measurements was established using a range of Certified Reference Materials, including HISS-1, NIST-1648a and NIST-1573a. The recoveries in these reference materials were 97.3-104.1% for aluminium. Total trace metal concentration was determined by adding leach and digest metal fractions. Total aluminium mass flux was used to calculate

lithogenic mass flux based on aluminium content of 7.1% in Saharan dust[55] and 7.7% in Patagonian dust[56] for NOG and SOG samples respectively. Stable nitrogen isotopic composition of sinking particulate nitrogen pool ($\delta^{15}N_{PN}$) was determined from $^{14}N/^{15}N$ mass ratio measured using Micro Cube elemental analyser (Elementar Analysensysteme GmbH, Hanau, Germany) interfaced to a PDZ Europa 20-20 isotope ratio mass spectrometer (Sercon Ltd., Cheshire, UK). The accuracy of the measurements was established using a set of laboratory standards calibrated against NIST Standard Reference Materials (IAEA-N1, IAEA-N2, IAEA-N3, USGS-40, and USGS-41). The analytical precision of the $\delta^{15}N_{PN}$ measurements was <0.1‰, while the difference between duplicates ranged between 3.1 and 11% (n=4). Measurements were performed at the UC Davies Stable Isotope Facility, USA.

Dust deposition flux. Direct and time-resolved measurements of dust deposition at NOG and SOG are not available. At SOG we obtained monthly estimates of dust deposition using an atmospheric model[14, 15], which utilizes reanalysis data (a combination of model and observations) to drive a dust chemical transport model, and was compared to long-term measurements of aerosol concentration. Dust deposition flux was modelled in four bins with the size distribution range of 0.1-0.5, 0.5-1.0, 1.0-2.5, and 2.5-10 μm. Dust deposition velocities were calculated within the model as a function of meteorological conditions and resulted in averages of 0.01, 0.029, 0.115, and 0.674 cm s^{-1} over our region. The modelled dust deposition fluxes were averaged for 3°×3° area centred at the SOG location. The uncertainty of the model output for the South Atlantic Ocean is hypothesised to be at least a factor of 10 due to scarcity and uncertainties in observational data and uncertainties in model source, transport and deposition processes[14]. Dust deposition flux at NOG was inferred from time-series dust concentrations measured over Barbados which is heavily influenced by air-masses from Sahara and Sahel deserts[13]. The details of dust sampling and processing are described in ref[13]. Dust

deposition flux was calculated by multiplying dust concentrations by a range of deposition velocities (0.01-1.2 cm s^{-1}) characteristic of relatively fine mineral dust aerosols of <5 µm in size typically arriving to the remote open ocean[57]. The resulting average dust deposition flux at NOG ranged from 0.085 to 10.2 mg m^{-2} s^{-1}. Assuming a deposition velocity of 1 cm s^{-1}, dust deposition flux is similar in magnitude to deep lithogenic flux at NOG. Thus, we considered this deposition velocity to be the most appropriate for calculations of daily dust deposition flux at NOG.

Upper ocean hydrography. Eight-day composite sea-surface temperature (SST) data were recorded by the Moderate Resolution Imaging Spectroradiometer (MODIS) sensor of NASA's Aqua satellite at 9 km resolution and averaged for 3°×3° box centred at each trap location. The annual cycle of mixed layer depth at the trap sites was derived from the ARGO-based climatology[58] averaged for 3°×3° area over the trap sites. The base of the mixed layer was defined as the depth at which the density was 0.03 kg m^{-3} less than that at 10 m.

Ancillary biogeochemical datasets were provided by the British Oceanographic Data Centre (BODC) and include vertical profiles of chlorophyll (archived data under accession numbers SOC050136 and SOC110235), nitrate concentrations (refs[59, 60] and archived dataset under accession number MIT130172), isotopic composition of total nitrate (refs[61, 62, 63]), nitrogen fixation rates (refs[22, 23, 24, 25]), ^{14}C-based primary production rates (ref[64] and archived data with accession numbers PP-PML090162, PP-PML110236 and PP-PML120146),

Primary production. Depth-integrated daily rates of primary production for the relevant time period were estimated from the chlorophyll-based eight-day resolved Vertically Generalized Production Model (VGPM)[16] and averaged for the 3°×3° area centred at the trap sites. The

VGPM data were downloaded from the Ocean Productivity website (http://www.science.oregonstate.edu/ocean.productivity/). Within relevant time periods, the VGPM-based productivity rates at NOG (160±14 mg C m^{-2} d^{-1}) and SOG (139±18 mg C m^{-2} d^{-1}) were comparable to the values measured directly at the trap sites in October-November 2008-2011 (240±96 mg C m^{-2} d^{-1} at NOG and 204±84 mg C m^{-2} d^{-1} at SOG (see ancillary biogeochemical datasets above).

Surface chlorophyll-*a* concentration. Eight-day composite surface chlorophyll-*a* data were recorded by MODIS Aqua at 9 km resolution and averaged for 3°×3° box centred at each trap location. MODIS Aqua calculates near-surface chlorophyll concentrations from a model of ocean colour using an empirical relationship.

Contribution of newly fixed nitrogen to the stable nitrogen isotope signal in trap material. The $\delta^{15}N$ of the trap material reflects both the autotrophic particle formation and the subsequent heterotrophic transformations. In the latter, the diagenetic fractionation can potentially alter $\delta^{15}N$ of the bulk nitrogen export and sequestration. No significant relationship was observed between C/N ratios and $\delta^{15}N$ of nitrogen export at NOG (r^2=0.02, n=12) while at SOG, this relationship was positive but weak and insignificant (r^2=0.25, n=12). This suggests that the observed variations in $\delta^{15}N$ of the trap material were determined predominantly during algal production, with no significant influence from detrital material and/or non-phytoplankton organisms[65]. At both sites isotopic fractionation following nitrogen assimilation is expected to be negligible due to constant nitrogen limitation in the surface waters[29]. Therefore, $\delta^{15}N$ of the produced organic matter should reflect the composition of dominating nitrogen sources to the euphotic zone, namely, upward diffusive flux of deep-water nitrate and N_2 fixation both having distinct isotopic signals. In addition, in the northern gyre, atmospheric dust deposition can

significantly contribute to the total pool of new nitrogen[31, 66]. Using equation (1) we describe isotopic composition of nitrogen export as mixing between diffused nitrogen from the upper thermocline and nitrogen from external source, represented by either diazotrophy or atmospheric deposition at NOG, and diazotrophy only at SOG:

$$\delta^{15}N_{PN} = (f_1 \times \delta^{15}N_{f1}) + (f_2 \times \delta^{15}N_{f2}) \quad (1)$$

where f_1 and f_2 and $\delta^{15}N$ denote fractions and isotopic signatures of dominant nitrogen sources. We estimate the percent contribution of these sources from a single choice of their respective endmember $\delta^{15}N$ values: +2.73‰ (NOG) and +6.22‰ (SOG) for nitrate diffusing from the shallow thermocline across the concentration gradient; -1.0‰ for N_2 fixation (both sites), -3.1‰ for bulk aerosol input (NOG only). Due to sensitivity of the two-endmember mixing model to the values of the chosen endmembers, we performed sensitivity analyses to account for uncertainty of the changing $\delta^{15}N$ endmembers on the fraction of $\delta^{15}N_{PN}$ (in %) originating from this source at each site, similar to isotopic assessment in ref[28]. The choices of $\delta^{15}N$ endmembers for each nitrogen source and those used in the sensitivity tests are described in the section below and the results are summarised in Supplementary Table 1.

Sensitivity analyses and $\delta^{15}N$ endmember choice.

Nitrate endmember: The choice of nitrate $\delta^{15}N$ endmember was based on the biogeochemical data (nitrate $\delta^{15}N$, nitrate and chlorophyll concentrations, PAR) obtained at the NOG and SOG sites during AMT cruises in May-June 2005 and October 2005, and US-GEOTRACES cruise GA03 in December 2011 (see ancillary biogeochemical datasets above).

At the permanently oligotrophic NOG and SOG sites, winter mixing is weak, and thermocline nitrate is supplied into the euphotic zone largely by turbulence-driven upward diffusion[67]. The magnitude of diffusive nitrate flux is governed by nitrate concentration gradients as the changes in turbulent diffusivity are relatively small[67]. At both sites, nitrate concentrations remain at

643 nanomolar levels (< 0.01 µmol L^{-1}) throughout the top 130-150 m and increase below,
644 signifying the position of the nitracline (defined by a nitrate concentration of 0.1 µmol L^{-1} (*e.g.*
645 ref[68]). The largest nitrate flux with a characteristic $\delta^{15}N$ signature is therefore expected at the
646 depth of the maximum nitrate concentration gradient typically found at depths near the base of
647 the euphotic zone (0.1 % surface PAR; includes the deep chlorophyll maximum).

648 Referring to vertical profiles of nitrate and chlorophyll concentrations, we calculate
649 concentration-weighted average nitrate $\delta^{15}N$ (ref[33]) from the top of the nitracline, where nitrate
650 concentrations begin to consistently increase, to the base of the euphotic zone. At NOG this
651 yields nitrate $\delta^{15}N$ of +2.73±0.36 ‰ (n=5) for the depth range of 137-191 m. In our isotopic
652 budgets this value represents an isotopic signal of nitrogen pool influenced by N_2 fixation and
653 atmospheric deposition, and sustained over time in the shallow thermocline. This is achieved
654 through both the internal cycle of low- $\delta^{15}N$ nitrate assimilation and subsequent
655 remineralisation and 2) accumulation of low- $\delta^{15}N$ nitrate imported during the northward water
656 mass transit[7, 30]. This nitrogen pool has not yet been homogenised with the large global ocean
657 nitrate reservoir (~4.8‰) or ^{15}N-enriched through denitrification[29, 30]. At SOG the most
658 relevant depth range for measured nitrate $\delta^{15}N$ spanned 226-230 m, substantially deeper than
659 the base of the euphotic zone. The corresponding mean $\delta^{15}N$ of +6.22±0.35‰ may thus
660 overestimate the value for the shallower waters, where preferential remineralisation of ^{14}N may
661 introduce a ^{15}N-depleted signal to the nitrogen pool[29].

662 For the primary sensitivity test (Supplementary Table 1) we used the minimal nitrate $\delta^{15}N$
663 observed in the upper thermocline at NOG (+0.96‰ at 137 m depth) to estimate the least
664 contribution of local N_2 fixation to $\delta^{15}N_{PN}$. We also tested nitrate $\delta^{15}N$ averaged from the top
665 of nitracline down to 26.8 kg m^{-3} isopycnal surface, which marks the main thermocline depth
666 at the study sites[7, 69]. The corresponding value at NOG was +3.53±0.40‰ (n=13) for the 136-

421 m depth range; the SOG value was +6.35±0.32 ‰ (n=3) for 226-306 m depth range. Finally, we included the oceanic global mean $\delta^{15}N$ (+4.8‰; ref[29]) to compare our isotope budgets with published data.

Nitrogen fixation endmember: We chose the mean $\delta^{15}N$ for diazotrophic biomass (-1±1‰) to represent the N_2 fixation endmember at both sites [29, 70, 71]. Assuming the mean nitrate $\delta^{15}N$ signal in the shallow thermocline, the range of the isotopic signal for diazotrophic nitrogen (-2‰ to 0‰) generates average contributions of 39.8-68.5% and 26.1-34.4% to $\delta^{15}N_{PN}$ at NOG and SOG, respectively (Supplementary Table 1).

Atmospheric deposition endmember: Atmospheric fluxes supply approximately ~9.9×10^9 mol N yr^{-1} to the central North Atlantic gyre and 5.8×10^9 mol N yr^{-1} to the South Atlantic gyre[72]. Although these values are notably smaller than regional estimates of new nitrogen inputs from diazotrophy (20×10^{11} mol N yr^{-1}; ref[73]), recent studies[30, 31, 35] suggest that deposition fluxes can significantly lower the $\delta^{15}N$ of the nitrogen pool. The published data on $\delta^{15}N$ in atmospheric fluxes in the open Atlantic Ocean is extremely scarce. Previous studies[31, 35, 74, 75, 76] report a wide range of $\delta^{15}N$ in bulk aerosol and rainfall samples (-6.8‰ to +1.7‰). Given that dry deposition dominates atmospheric input at NOG, a value close to an average isotopic signal of bulk aerosols seems the most appropriate to represent the dust endmember at NOG. We thus choose $\delta^{15}N$ of -3.1‰, based on the mean $\delta^{15}N$ values measured in the Sahara-influenced aerosol samples collected the sub-tropical North Atlantic[31, 74] and Crete[76]. For the sensitivity test, we varied $\delta^{15}N$ of aerosol N across the full range, also including annual (-4.5‰) and seasonal cold (-6.8‰; October-March) and warm (-1.9‰; April-September) averages measured in the Bermuda rainfall[35, 74, 75] (Supplementary Table 1). We find that with the nitrate $\delta^{15}N$ of 2.73‰, aerosol nitrogen can account for a sizable fraction of $\delta^{15}N$ of nitrogen export at NOG (21.7-176%). Therefore, with nitrogen input equal or greater to magnitude of N_2 fixation, dust deposition can have a similar or greater effect on the isotopic budget of trap

material from NOG. Hence, future studies should include the measurements of both magnitude and $\delta^{15}N$ of dust deposition and N_2 fixation to avoid under- or over-estimation of the importance of each of source.

Assessment of ballast effect of lithogenic flux. We examined the relationship between POC and (bio)mineral at NOG and SOG using POC flux model by ref[2] . The model divides POC flux into fractions ballasted by biomineral (opal + calcite; POC_{bio}) and lithogenic (POC_{lith}) particles, and freely sinking POC (POC_{free}). We use multiple linear regression to fit the particle flux data into equation (2) and determine correlation coefficients *a*, *b* and *c* (hereafter, carrying coefficients) for each fraction, following approach in refs[2, 42, 77].

$$\text{POC flux} = a \times POC_{bio} + b \times POC_{lith} + c \times POC_{free} \quad (2)$$

Carrying coefficients only reflect the size of the ballast-normalized fraction of POC flux, but not their absolute magnitudes, and are used to calculate the relative fraction (in %) of POC associated with each ballast type[42, 77]. We further assume that the POC_{free} fraction is negligible at 3000 m depth and force multiple linear regression to pass through zero[2]. The strong temporal variability of dust deposition limits the relevance of the annual-scale approach for estimating the role of lithogenic ballast to POC flux. Hence, we first assess the effect of lithogenic ballast based on different POC sequestration scenarios, namely, (1) elevated POC flux (≥120% of annual mean) at NOG, (2) POC flux at NOG outside scenario (1), (3) POC flux at SOG. We evaluated the sensitivity of these results by performing multiple linear regression on the NOG flux dataset separated according to the high and low lithogenic fluxes (Supplementary Table 2). Our approach differs from that applied previously by refs[2, 42, 77] in which carrying coefficients for both calcite and opal were determined. This is due to strong collinearity observed between calcite and opal in all POC-based groups, violating the independence assumption of multiple linear regression, as further determined by ridge regression analysis. The resulting carrying coefficients and calculated proportion of ballast-associated POC flux in

each surveyed group are summarised in Supplementary Table 2. The carrying coefficients for lithogenic material compared well with the global and the north Atlantic means (0.052, and 0.058, respectively)[2] during low POC flux, but exceeded these values during high fluxes and overall at SOG. We acknowledge that the relatively large carrying coefficient for lithogenic ballast in the SOG group compared to the NOG groups and other time-series might be an overestimation introduced by a nearly 1:1 ratio between POC and lithogenic fluxes and a their strong positive correlation (Spearman's p = 0.91). As a result, the proportion of POC flux ballasted by lithogenic material appears to be comparable between SOG and scenario (2) at NOG, despite the significant difference in their lithogenic fluxes (Supplementary Table 2).

Data availability: The data analysed during this study are available from the corresponding author upon reasonable request. The supporting data for this study are available from the repository of the British Oceanographic Data Centre upon request.

51. Hedges, J.I., Stern, J.H. Carbon and nitrogen determinations of carbonate-containing solids1. *Limnol. Oceanogr.* **29**(3)**:** 657-663 (1984).

52. Salter, I., Lampitt, R.S., Sanders, R., Poulton, A., Kemp, A.E., Boorman, B., *et al.* Estimating carbon, silica and diatom export from a naturally fertilised phytoplankton bloom in the Southern Ocean using PELAGRA: a novel drifting sediment trap. *Deep-Sea Res. Pt. II.* **54**(18)**:** 2233-2259 (2007).

53. Mortlock, R.A., Froelich, P. N. A simple method for the rapid determination of biogenic opal in pelagic marine sediments. *Deep-Sea Res.* **36**(9)**:** 1415-1426 (1989).

54. Planquette, H., Fones, G.R., Statham, P.J., Morris, P.J. Origin of iron and aluminium in large particles (> 53 μm) in the Crozet region, Southern Ocean. *Mar. Chem.* **115**(1)**:** 31-42 (2009).

55. Guieu, C., Loÿe-Pilot, M.D., Ridame, C., Thomas, C. Chemical characterization of the Saharan dust end-member: Some biogeochemical implications for the western Mediterranean Sea. *J. Geophys. Res.-Atmos. (1984–2012)* **107**(D15)**:** ACH 5-1-ACH 5-11 (2002).

56. Gaiero, D.M., Probst, J.-L., Depetris, P.J., Bidart, S.M., Leleyter, L. Iron and other transition metals in Patagonian riverborne and windborne materials: geochemical control and transport to the southern South Atlantic Ocean. *Geochim. Cosmochim. Ac.* **67**(19)**:** 3603-3623 (2003).

57. Torres-Padrón, M., Gelado-Caballero, M., Collado-Sánchez, C., Siruela-Matos, V., Cardona-Castellano, P., Hernández-Brito, J. Variability of dust inputs to the CANIGO zone. *Deep-Sea Res.* **49**(17)**:** 3455-3464 (2002).

58. Hosoda, S., Ohira, T., Sato, K., Suga, T. Improved description of global mixed-layer depth using Argo profiling floats. *J. Oceanogr.* **66**(6)**:** 773-787 (2010).

59. Harris, C., Woodward E.M.S., AMT20 (JC053) micro-molar nutrient measurements from CTD bottle samples. British Oceanographic Data Centre - Natural Environment Research Council, UK (2014). doi:10.5285/f3c482e3-245e-36a5-e044-000b5de50f38.

60. Harris, C.; Rees, A. AMT19 (JC039) micro-molar nutrient measurements from CTD bottle samples. British Oceanographic Data Centre - Natural Environment Research Council, UK (2016). doi:10.5285/42974c1c-ea2d-57a5-e053-6c86abc09d06

61. Casciotti, K., McIlvin, M.R., Forbes, M.S., Sigman D. Nitrate isotopes of nitrate in the GEOTRACES North Atantic Zonal Transect – laboratory Casciotti, British Oceanographic Data Centre - Natural Environment Research Council, UK (2016). doi:10.5285/2317515c-05c1-6d14-e053-6c86abc0690e.

62. Casciotti, K. Nitrogen and oxygen isotope measurements of nitrate from CTD bottles during cruise AMT16 (D294). British Oceanographic Data Centre - Natural Environment Research Council, UK (2015). doi:10.5285/1d4233e0-58e4-637e-e053-6c86abc0ad64.

63. Weigand, A., Marconi, D., Sigman, D., Casciotti, K. Nitrate isotopes of nitrate in the US GEOTRACES North Atlantic Zonal Transect – laboratory Sigman, British Oceanographic Data Centre - Natural Environment Research Council, UK (2016). doi:10.5285/2317515c-05c0-6d14-e053-6c86abc0690e.

64. Widdicombe, C., Tilstone, G., Rees, A. AMT19 (JC039) Primary Production (Size-fractionated) incubations using ^{14}C uptake from CTD bottle samples. British Oceanographic Data Centre - Natural Environment Research Council, UK (2015). doi:10.5285/1feecc3c-a422-5d7d-e053-6c86abc0435d.

65. Waser, N.A.D., Harrison, W.G., Head, E.J.H., Nielsen, B., Lutz, V.A.E., Calvert, S. Geographic variations in the nitrogen isotope composition of surface particulate nitrogen and new production across the North Atlantic Ocean. *Deep-Sea Res. Pt. I* **47**(7)**:** 1207-1226 (2000).

66. Baker, A., Kelly, S., Biswas, K., Witt, M., Jickells, T. Atmospheric deposition of nutrients to the Atlantic Ocean. *Geophys. Res. Lett.* **30**(24) (2003).

67. Lewis, M.R., Harrison, W.G., Oakey, N.S., Herbert, D., Platt, T. Vertical nitrate fluxes in the oligotrophic ocean. *Science* **234**(4778)**:** 870-872 (1986).

68. Painter, S.C., Patey, M.D., Forryan, A., Torres-Valdes, S. Evaluating the balance between vertical diffusive nitrate supply and nitrogen fixation with reference to nitrate uptake in the eastern subtropical North Atlantic Ocean. *J. Geophys. Res.-Oceans* **118**(10)**:** 5732-5749 (2013).

69. Marconi, D., Weigand, M.A., Rafter, P.A., McIlvin, M.R., Forbes, M., Casciotti, K.L., et al. Nitrate isotope distributions on the US GEOTRACES North Atlantic cross-basin

section: Signals of polar nitrate sources and low latitude nitrogen cycling. *Mar. Chem.* 177: 143-156 (2015).

70. Carpenter, E.J., Harvey, H.R., Fry, B., Capone, D.G. Biogeochemical tracers of the marine cyanobacterium Trichodesmium. *Deep-Sea Res. Pt. I* **44**(1)**:** 27-38 (1997).

71. Mahaffey, C., Williams, R.G., Wolff, G.A., Anderson, W.T. Physical supply of nitrogen to phytoplankton in the Atlantic Ocean. *Glob. Biogeochem. Cycles* **18**(1) (2004).

72. Baker, A.R., Lesworth, T., Adams, C., Jickells, T.D., Ganzeveld, L. Estimation of atmospheric nutrient inputs to the Atlantic Ocean from 50°N to 50°S based on large-scale field sampling: Fixed nitrogen and dry deposition of phosphorus. *Glob. Biogeochem. Cycles* **24**(3)**:** GB3006 (2010).

73. Gruber, N. & Sarmiento, J. L. Global patterns of marine nitrogen fixation and denitrification. *Glob. Biogeochem. Cycles* 11, 235-266 (1997).

74. Gobel, A.R., Altieri, K.E., Peters, A.J., Hastings, M.G., Sigman, D.M. Insights into anthropogenic nitrogen deposition to the North Atlantic investigated using the isotopic composition of aerosol and rainwater nitrate. *Geophys. Res. Lett.* **40**(22)**:** 5977-5982 (2013).

75. Hastings, M.G., Sigman, D.M., Lipschultz, F. Isotopic evidence for source changes of nitrate in rain at Bermuda. *J. Geophys. Res.-Atmos.* **108**(D24) (2003).

76. Mara, P., Mihalopoulos, N., Gogou, A., Daehnke, K., Schlarbaum, T., Emeis, K.C., *et al.* Isotopic composition of nitrate in wet and dry atmospheric deposition on Crete in the eastern Mediterranean Sea. *Glob. Biogeochem. Cycles* **23**(4) (2009).

77. Le Moigne, F.A., Sanders, R.J, Villa-Alfageme, M., Martin, A.P., Pabortsava, K., Planquette, H., *et al.* On the proportion of ballast versus non-ballast associated carbon export in the surface ocean. *Geophys. Res. Lett.* **39**(15) (2012).

841 **FIGURES**

842 **Figure 1**

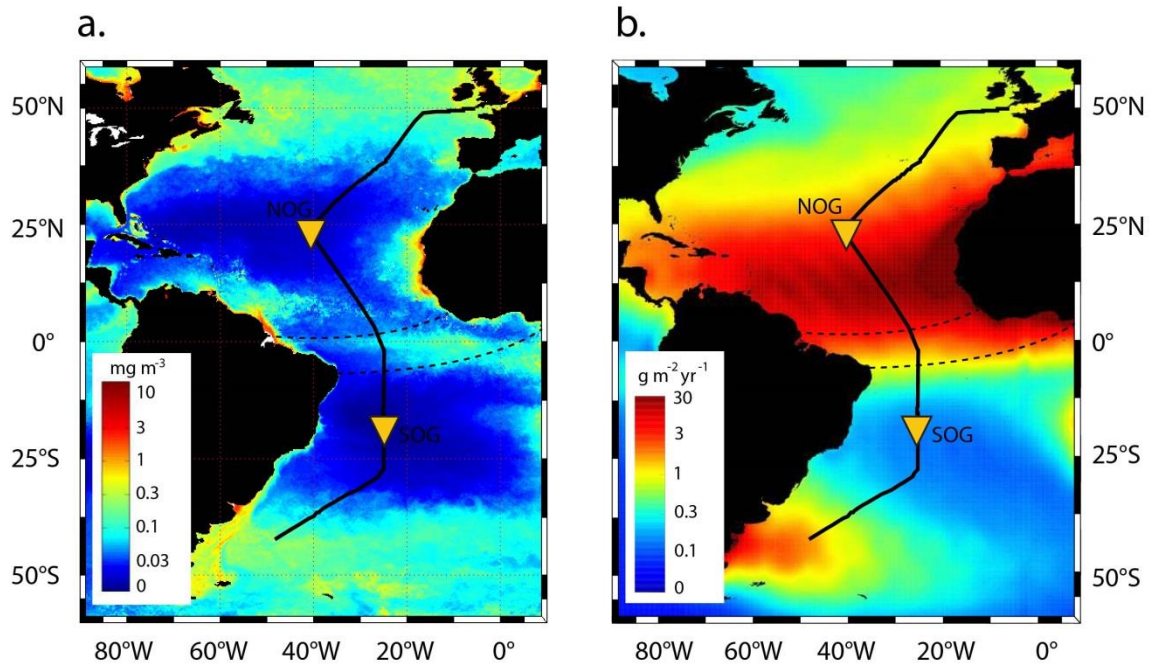

843

844

Figure 2

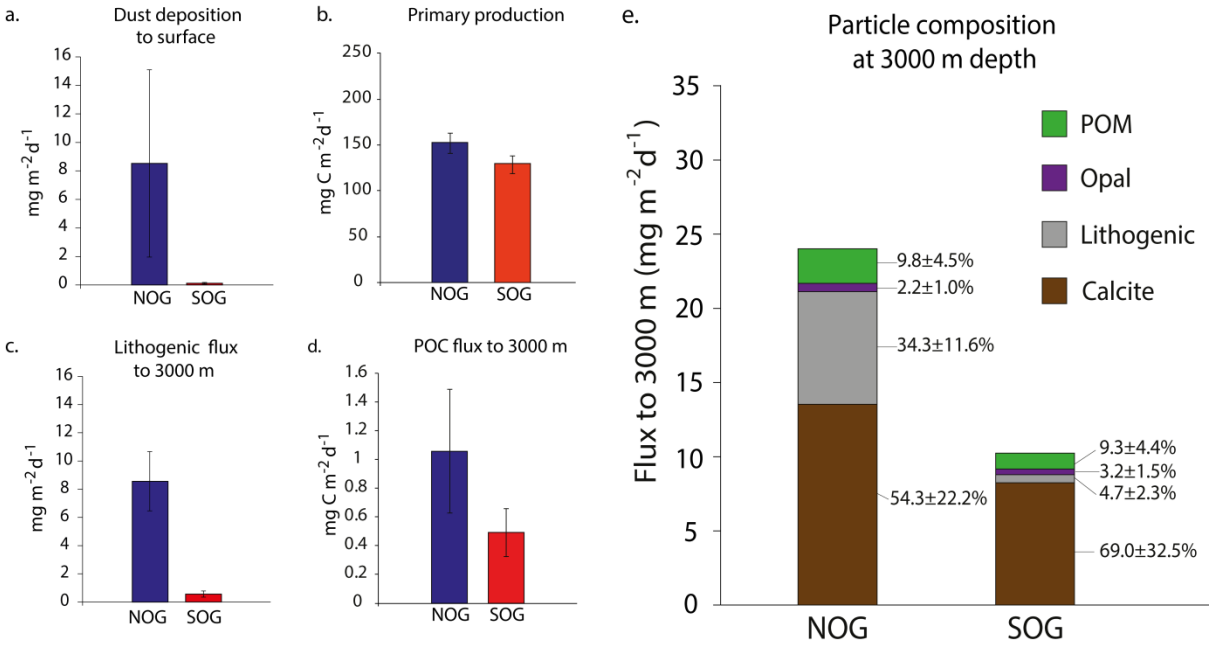
a.
Dust deposition to surface
mg m-2d-1
NOG
SOG
b.
Primary production
mg C m-2d-1
c.
Lithogenic flux to 3000 m
d.
POC flux to 3000 m
e.
Particle composition at 3000 m depth
Flux to 3000 m (mg m-2d-1)
POM
Opal
Lithogenic
Calcite
9.8±4.5%
2.2±1.0%
34.3±11.6%
54.3±22.2%
9.3±4.4%
3.2±1.5%
4.7±2.3%
69.0±32.5%

848 **Figure 3**

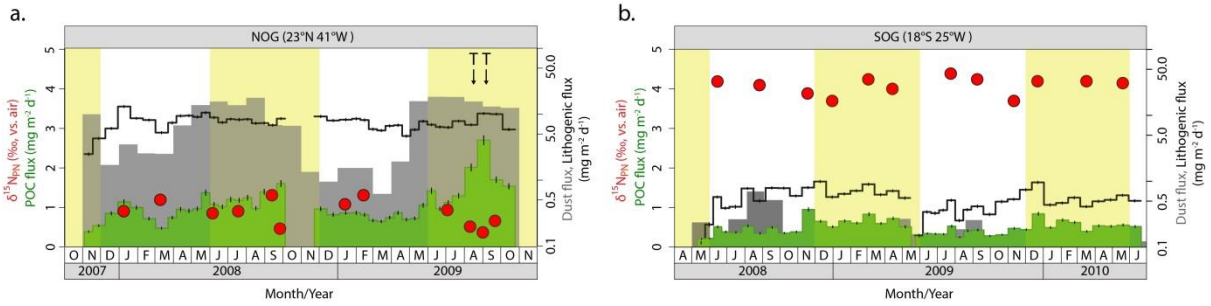

849

850

Figure 4

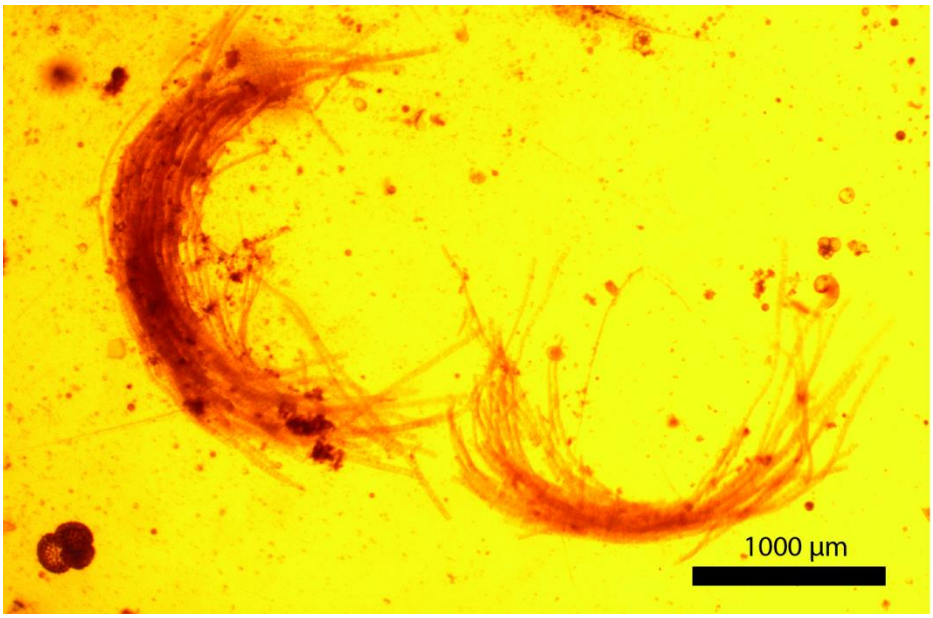

Figure 5

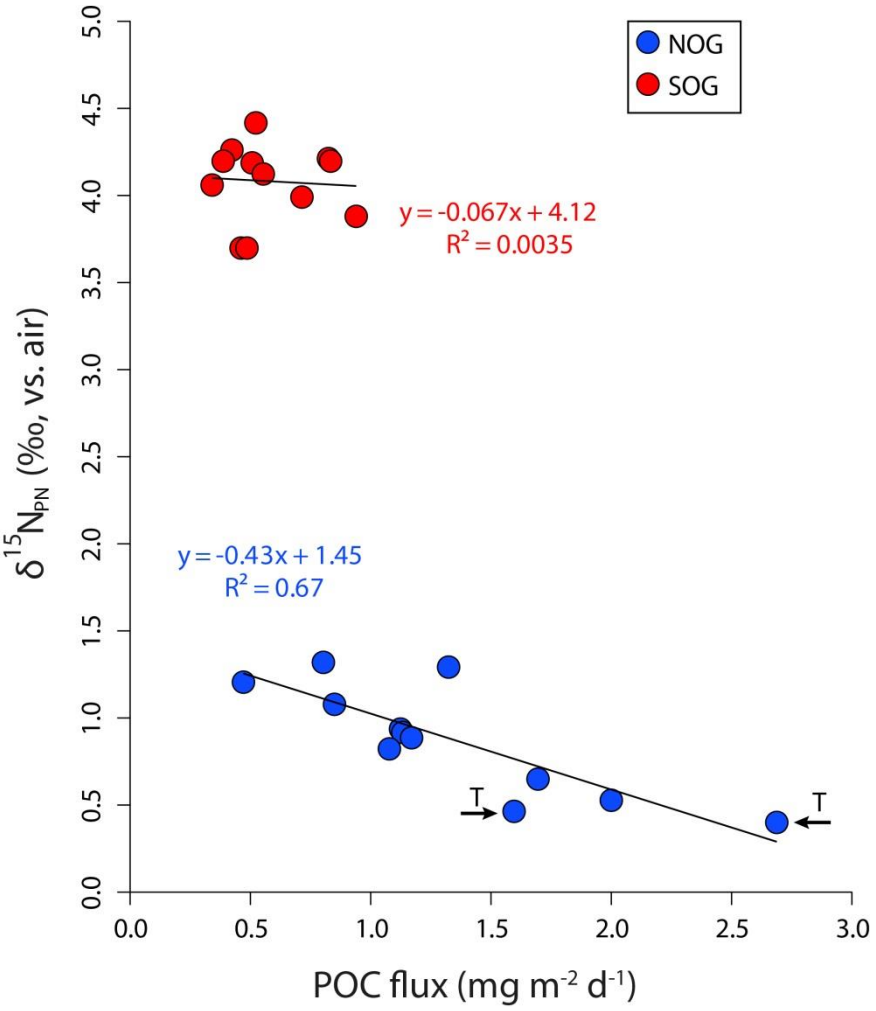
NOG
SOG
y = -0.067x + 4.12
R² = 0.0035
y = -0.43x + 1.45
R² = 0.67
T
T
δ15NPN (‰, vs. air)
POC flux (mg m-2 d-1)
0.0
0.5
1.0
1.5
2.0
2.5
3.0
3.5
4.0
4.5
5.0

SUPPLEMENTARY INFORMATION

Supplementary Table 1| Sensitivity analysis of the choice endmember $\delta^{15}N$ value on calculated source contribution (%) to isotopic signal of nitrogen flux at 3000 m depth

Nitrate endmember $\delta^{15}N$ (‰)	N_2 fixation (%)			Dry deposition (%)			Rainfall (%)		
	Min	Choice	Max	Min	Choice	Max	Min	Choice	Max
NOG	*-2*	*-1*	*0*	*-6*	*-3.1*	*+1.7*	*-6.8*	*-4.5*	*-1.9*
+0.96 (min NOG)	2.82	4.25	8.68	1.20	2.1	-11.3	1.07	1.53	2.91
+2.73 (137- 191 m)	**39.8**	**50.4**	**68.5**	**21.7**	**32.4**	**176.2**	**19.8**	**26.2**	**40.7**
+3.53 (137-421 m)	48.0	58.6	75.2	27.4	40.0	145.0	25.7	33.0	48.9
+4.8*	57.7	67.7	81.7	36.3	49.7	126.6	33.8	42.2	58.6
SOG	*-2*	*-1*	*0*						
+6.22 (226-230 m)	**26.1**	**29.7**	**34.4**						
+6.35 (226-306 m)	27.2	30.9	35.8						
+4.8*	10.6	12.5	15.1						

The source and choice of $\delta^{15}N$ endmember values are described in Methods. Depth-range over which measured nitrate $\delta^{15}N$ values were averaged (nitrate concentration weighted) is given in parentheses. Bold values show the percentage contribution values calculated with the preferred endmember $\delta^{15}N$ values.

*global average $\delta^{15}N$ of deep-water nitrate (ref[29])

863 **Supplementary Table 2| Results of multiple linear regression model**

Group	Mean flux (mg m^{-2} d^{-1})			Carrying coefficient*		Ballasted POC flux (%)		$R^{2‡}$
	POC	Opal + Calcite	Lithogenic	Opal + Calcite	Lithogenic	Opal + Calcite	Lithogenic	
NOG groups								
High POC (10)	1.64±0.43	17.4±6.7	9.14±1.9	0.027^{ns}	0.126	29.1	70.1	0.94
Low POC (31)	0.88±0.21	13.0±3.5	8.38±2.2	0.036	0.048	53.7	45.7	0.98
High Lith (9)	1.31±0.58	15.6±1.81	11.3±1.44	0.067 ^{ns}	0.025 ^{ns}	79.7	21.2	0.87
Low Lith (32)	0.99±0.36	13.7±5.27	7.80±1.62	0.045	0.048	62.3	37.6	0.95
SOG group (40)	0.49±0.17	8.62±2.96	0.54±0.21	0.032	0.371	57.2	41.0	0.96

Values in parentheses indicate number of data points (=collection cups) pulled into each group. Statistically not significant carrying coefficients ($p>0.01$) are marked with 'ns'.

* Correlation coefficients of multiple linear regression determined from equation (2) (see Methods).

‡ Overall model fit

864

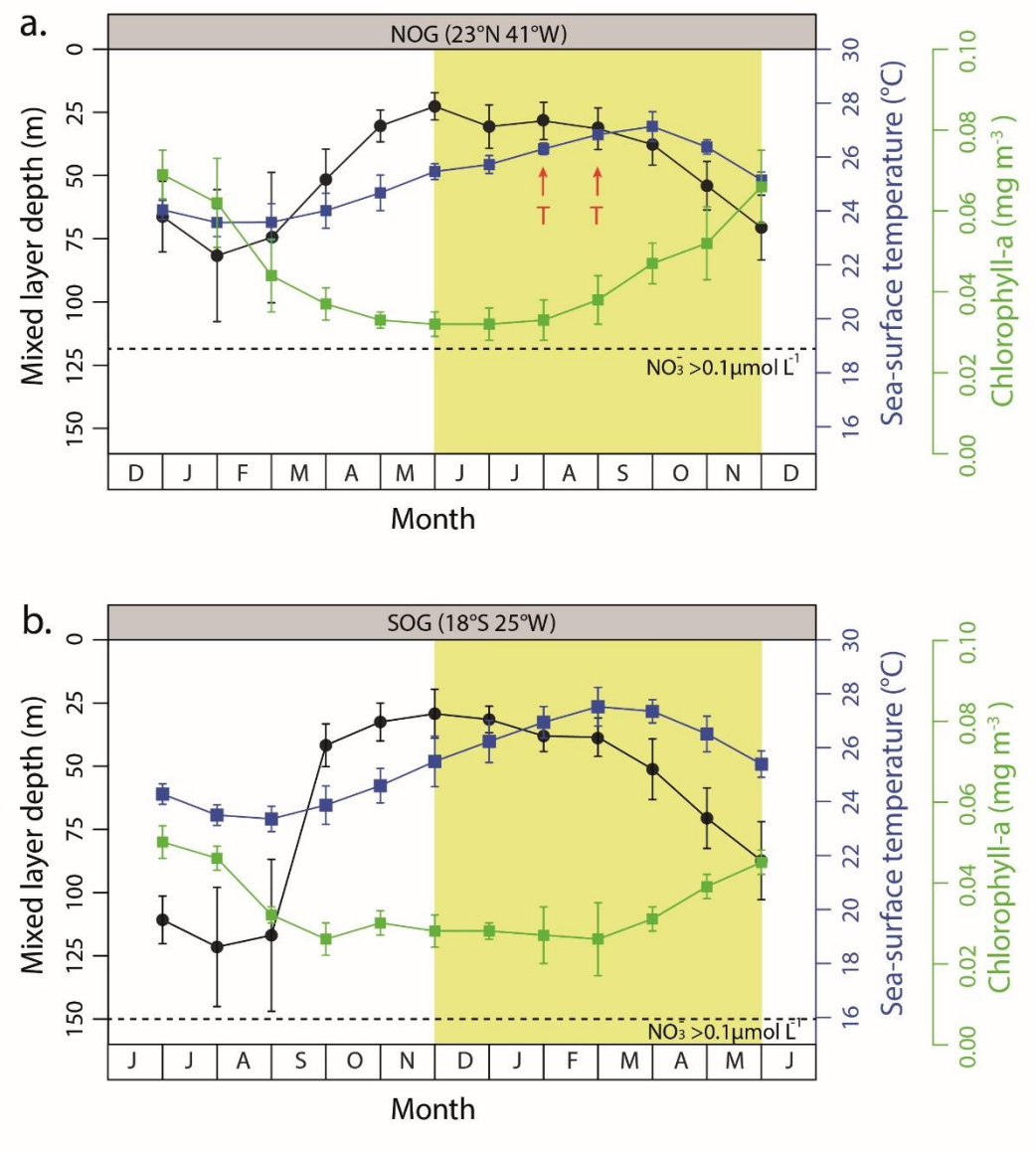

865

866 **Supplementary Figure 1| Annual cycle of sea-surface temperature, mixed layer depth and**
867 **surface chlorophyll-*a* at NOG (a) and SOG (b).** Monthly-averaged sea-surface temperature
868 and chlorophyll-a concentrations are recorded by the MODIS-A satellite at 9km resolution
869 during 2007-2010. Error bars show one standard deviation of the temporal mean. The mixed
870 layer depth is derived from the ARGO-based climatology. Error bars show one standard
871 deviation of the areal mean. In **a** and **b**, dashed line indicates the approximate depth of
872 nutricline ($\mathbf{NO_3^-}$>0.1µmol L^{-1}), based on *in situ* nitrate measurements during AMT cruises 18-
873 21 in October-November 2008-2010 (see Methods for data sources). In **a,** red letter "T" point
874 to the months, when *Trichodesmium* "tufts" were recovered in the NOG traps.

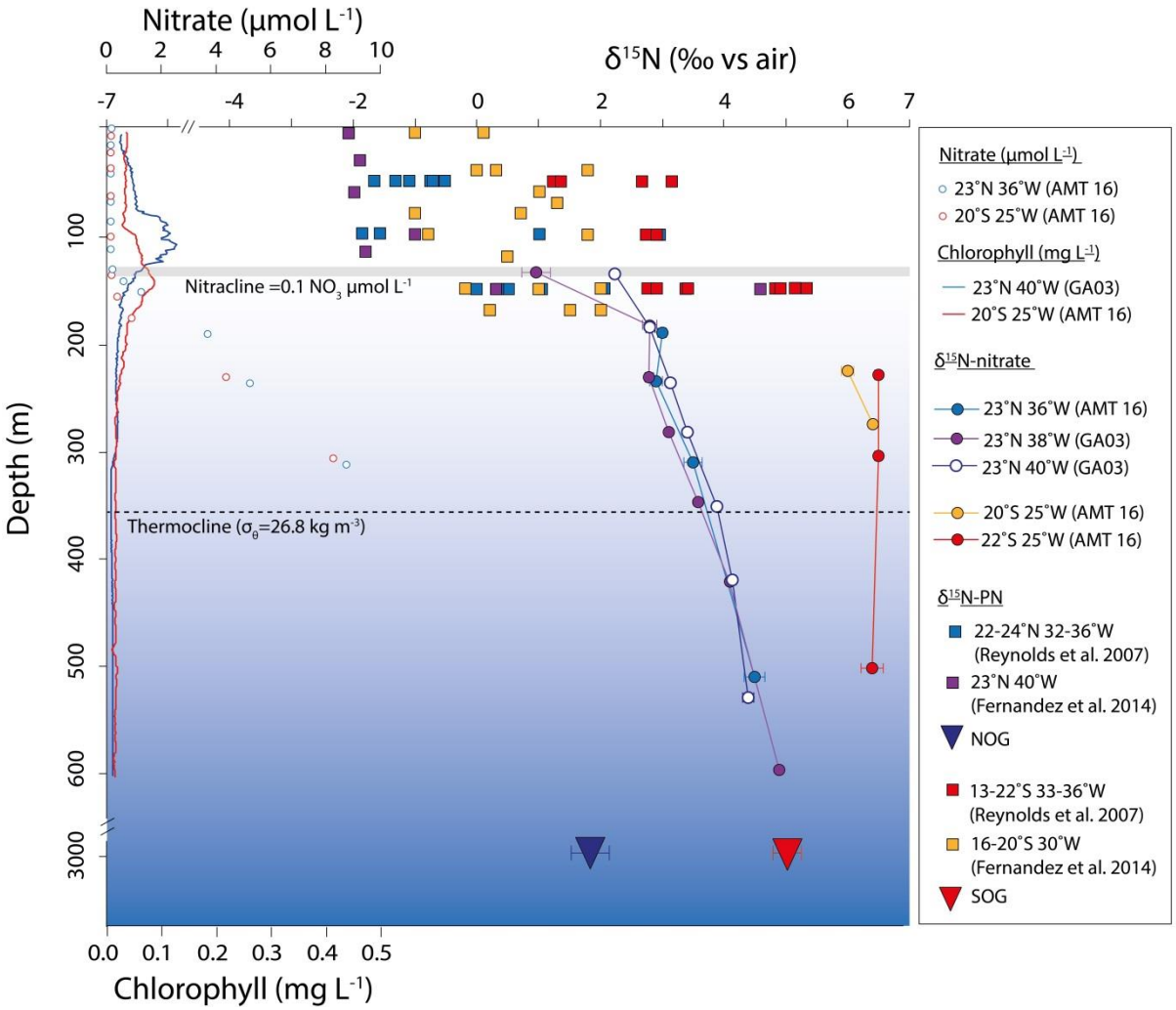

Supplementary Figure 2| Nitrogen isotope data for water column total nitrate, suspended particles and trap material near the study. Concentrations of nitrate and chlorophyll measured at the study sites are also shown. Data sources are described in the figure legend with complete references provided in the Methods section.